Journal of Applied Polymer Science

Non-Isothermal Crystallization Kinetics and Morphology of Mica Particles Filled Biodegradable Poly(butylene succinate)

Ning Zhang,[1,2] Jinping Qu,[1,2] Bin Tan,[1,2] Xiang Lu,[1,2] Jintao Huang,[1,2] Guizhen Zhang,[1,2] Yongqing Zhao,[1,2] Gang Jin[1,2]

[1]National Engineering Research Center of Novel Equipment for Polymer Processing, South China University of Technology, Guangzhou 510640, People's Republic of China

[2]Key Laboratory of Polymer Processing Engineering of Ministry of Education, South China University of Technology, Guangzhou 510640, People's Republic of China

Correspondence to: J.-P. Qu (E-mail: jpqu@scut.edu.cn); G. Jin (E-mail: pmrdd@scut.edu.cn)

ABSTRACT: Biodegradable poly(butylene succinate) (PBS)/mica composites were prepared by melt blending. The non-isothermal crystallization kinetics, spherulitic morphology, and crystalline structure were investigated by DSC, POM, and WAXD, respectively. The concepts of ''crystallization rate coefficient" and ''crystallization rate parameter" were employed. The non-isothermal crystallization behavior was successfully analyzed by Avrami and Liu methods while the Ozawa method failed to describe it. The WAXD and POM results showed that the addition of mica did not alter the crystalline structure, but increased the number of nuclei and reduced the size of the spherulites. In addition, the activation energy was also obtained from Hoffman–Lauritzen theory. These results showed that the addition of mica into PBS matrix played a dual role: they acted as nucleation agents to promote the process of nucleation, while acted as physical impediments to retard the growth of crystal. The former was dominating as the crystallization rates of mica/PBS composites were accelerated. © 2013 Wiley Periodicals, Inc. J. Appl. Polym. Sci. 130: 2544–2556, 2013

KEYWORDS: crystallization; composites; kinetics

Received 9 February 2013; accepted 26 April 2013; Published online 27 May 2013
DOI: 10.1002/app.39469

INTRODUCTION

During the last two decades, researches focused on biodegradable polymers with good practical properties have aroused more and more important attentions from many countries and regions, due to the potential application and environmental consideration.[1–3] These environment friendly polymers can be degraded easily into carbon dioxide and humus in the suitable environmental conditions.[4,5] The most promising biodegradable polymeric materials are aliphatic polyesters, among which poly(butylene succinate) (PBS) is a widely used and highly practical biodegradable polymer.[36–9] PBS is the focus of many areas, due to its good characteristics, including high biodegradability, practical process ability, and stable thermal properties.[6,10] It is a white crystalline thermoplastic, with a fusing point approximate to low density polyethylene.[9,11] Many papers about the structure, spherulitic morphology, crystallization behavior, crystallization kinetics, and mechanical properties of PBS have been published.[12–18]

However, a wide range of utilizations for PBS has been restricted due to its defects including softness, high cost and so on.[13] To overcome these shortcomings, blending PBS with the other materials is one of the commonly used methods, especially, blending with inorganic particles which may not only improve the mechanical properties, but also lower the cost.[6,19,20] Okamoto and co-workers[21,22] had blended PBS with montmorillonite (C18-mmt), and they found that the mechanical properties of the composites were improved greatly.

Muscovite mica is an interesting kind of layered aluminosilicate with many good properties and its formula is $K_2Al_4(Al_2Si_6O_{20})(OH)_4$.[23] As mica has many interesting characteristics, such as the high heat stability, the high aspect ratio (ratio of diameter to thickness), the effect of two-dimensional reinforcing, the high swelling capacity, the high water-absorbing properties, the outstanding corona resistance and insulation properties, the low overall cost, the easiness in production, and the friendliness to the environment, many authors have studied composites with the addition of mica.[23–32] Gan et al.[26] had reported that the coefficient of friction and wearing rate of mica/PAEK composites were affected by the amount of mica used. Okamoto et al.[33,34] had blended PLA with synthetic fluorine mica, and

they found that the mechanical properties of the composites were also improved greatly.

Obviously it is very interesting to make researches on blending of biodegradable polymeric materials with mica from both academic and industrial perspectives of view, because of the possibilities for enhancing mechanical properties and thermal stability of biodegradable polymers, and reducing the material cost as well as extending their practical application. For PBS composites, however, there are only a few reports on PBS composites filled with mica.[34] As we know, mechanical properties, biodegradable properties and thermal properties are greatly influenced by crystallization behavior and kinetics related to the thermal process.[35,36] Therefore, to better understand the relationship between mica and its PBS composites, characterize materials, and optimize processing parameters, the crystal structure, the crystallization kinetics and crystallization morphology should be studied, especially in the non-isothermal crystallization process for the reason that the non-isothermal conditions is of meaningful practical significance.[13,37] In this investigation, mica/PBS composites were obtained by melt-compounding process. The purpose of this study is to understand the effect of the mica particles on the spherulitic morphology, crystalline structure, crystallization behavior and non-isothermal crystallization kinetics of neat PBS in the non-isothermal processes. The non-isothermal crystallization kinetics of mica/PBS composites with different contents of mica have been studied by applying three kinds of models in detail, including Avrami model, Ozawa model, and combined Avrami–Ozawa model. Moreover, the activation energies of non-isothermal crystallization for pure PBS and its composites were also studied in this article.

EXPERIMENTAL

Materials and Sample Preparation

The PBS (Bionolle® 1020) for the blending process was bought from Showa Polymer Co. (Japan). The molecular weight of this PBS was 60,000, the density of it was 1.26 g/cm^3, and the melt flow index was 25 g/10 min at the temperature of 190°C under the weight of 2.16 kg.

The white mica powder (1250#) was purchased from Chuzhou great mining company (People's Republic of China). The mica pellets were about 10 μm in diameter.

First, PBS and mica powder were dried in a sealed vacuum condition at the temperature of 40°C for more than 8 h to get rid of the moisture. Then the neat PBS was melt compounded with mica particles (0, 1, 2, 4, and 8 wt %, respectively) in a Brabender mixer (Germany) at 153°C for about 10 min at the screw speed of 80 rounds per minute (rpm). The SEM (scanning election microscopy) picture of the composite with 4% of mica particles was shown in Figure 1. The mica particles were well dispersed in the polymer matrix.

Differential Scanning Calorimetry (DSC)

Non-isothermal crystallization kinetics for neat PBS and its composites was obtained under the DSC equipment. The model of the DSC equipment is 204c (Netzsch, Germany) and a liquid nitrogen-cooling accessory was equipped for the non-isothermal crystallization process. The sensitivity for calorimetric process of this device was about 3.0–4.5 mV/mW, and the precision error of it was less or equal than 0.1 K. The samples with the weight of about 5 mg were sealed in a plate which is made of aluminum. All the samples were first heated from room temperature to 160°C at the rate of 30°C/min in the nitrogen atmosphere condition, and then the temperature was held for 5 min to get rid of the thermal history of the specimens. Finally, the samples were cooled at different constant rates of 30, 20, 10, and 5°C/min. We investigated the recorded exothermal flow curves for non-isothermal crystallization kinetics at different cooling rates.

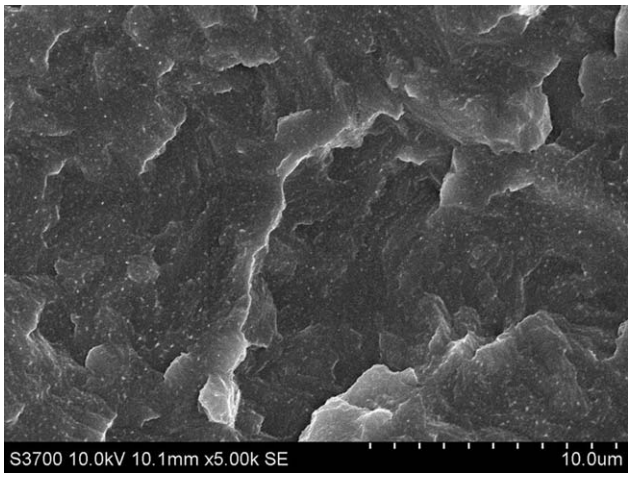

Figure 1. SEM micrograph of mica/PBS (4/96) composite.

Wide-Angle X-ray Diffraction (WAXD)

For wide-angle X-ray diffraction (WAXD) analysis, neat PBS, mica, and mica/PBS composites were studied by a D8 ADVANCE (Bruker, Germany). The working condition for the instrument is at both 40 mA and 40 kV, with the radiation of Cu $K\alpha$. We obtain the scans between Bragg angles with the range of 5–60° at a constant rate of 2° per min.

Polarizing Optical Microscopy (POM)

An Axioskop-40POL (Germay) polarizing optical microscopy (POM) equipped with a CCD camera was used to observe the morphology of pure PBS and its composites. A small fragment of the samples was put on a heating stage between two microscope cover glasses. All the specimens were heated from room temperature to 160°C, and then the temperature was held for 5 min to get rid of the thermal history. Then, all the specimens were cooled to room temperature by the natural cooling. Finally, we obtain the spherulite morphology of pure PBS and its composites after the crystallization process. All the samples were placed on the heating stage through the whole procedure without moving.

RESULTS AND DISCUSSION

Non-isothermal Crystallization Behavior

As most plastic processing are operated in the non-isothermal conditions, the investigation of the non-isothermal crystallization behavior is very important.[13,37] The crystallization behavior of the non-isothermal process for pure PBS and its composites was investigated at different constant cooling rates from 5 to 30°C/min. The crystallization exotherms of pure PBS and mica/PBS

Applied Polymer SCIENCE

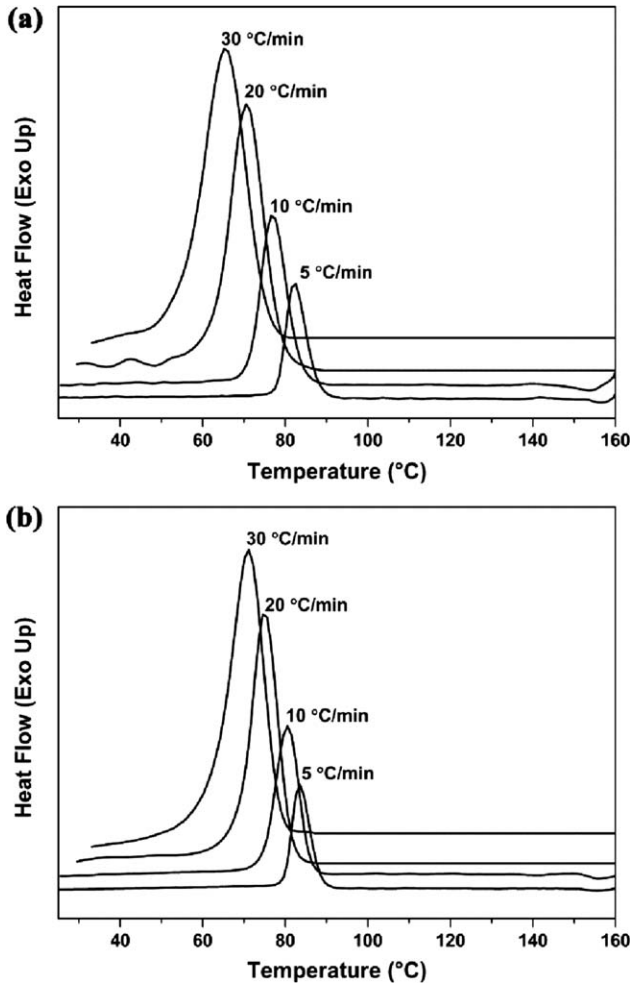

Figure 2. DSC curves of non-isothermal melt crystallization for (a) neat PBS and (b) mica/PBS (4/96) composite at the indicated cooling rates.

(4/96) composite for non-isothermal crystallization at different constant cooling rates were shown in Figure 2. The crystallization peak temperature (T_p), the onset temperature (T_0), the crystallization enthalpy (ΔH_c), and the other parameters for the non-isothermal process got from these exothermic curves under different constant cooling rates were summarized in Table I.

Crystallization Peak Temperature. For all the samples, the onset temperature of crystallization T_0 and the crystallization peak T_p had a trend of shifting to a lower temperature and the temperature range became broader with the increase of the cooling rate. The trend of shift for T_p to a relative lower temperature indicates that the crystallization happens earlier when the cooling rate is lower. As the specimens were cooled with lower cooling rates, the time for the nucleation was enough; thus, the crystallization process can occur earlier with a relative higher temperature. In contrast, when the samples were cooled at a higher cooling rate, the time for the crystallization process was not enough and the motion for the PBS chains cannot match the cooling rate. Thus, bigger supercooling for the crystallization process was needed with a relative higher cooling rate, indicating the fact that the crystallization peak T_p had a trend of shifting to a lower temperature and the crystallization

Table I. Non-isothermal Crystallization Parameters T_p, T_0, ΔH_C, and $t_{1/2}$ for Neat PBS and Mica/PBS Composites at Δifferent Cooling Rates

Sample	φ (°C/min)	T_p (°C)	T_0 (°C)	ΔH_c (J/g)	$t_{1/2}$ (min)
PBS	5	82.2	87.6	67.33	2.38
	10	76.9	83.4	65.66	1.43
	20	70.6	78.5	68.67	0.91
	30	65.3	74.7	63.09	0.54
Mica/PBS(1/99)	5	83.8	88.5	69.18	1.90
	10	78.9	84.6	69.32	1.20
	20	73.3	80.2	68.48	0.70
	30	69.1	76.5	61.18	0.40
Mica/PBS(2/98)	5	83.7	88.6	69.82	1.90
	10	78.3	84.7	67.34	1.19
	20	73.7	80.9	68.63	0.62
	30	69.9	77.3	61.13	0.40
Mica/PBS(4/96)	5	83.5	88.4	68.98	1.94
	10	80.6	85.8	64.62	1.07
	20	75.1	81.4	65.39	0.59
	30	71.2	78.3	61.21	0.39
Mica/PBS(8/92)	5	85.1	89.3	64.4	1.74
	10	80.7	85.6	65.67	0.96
	20	76.2	82.4	62.26	0.54
	30	72.7	79.8	58.35	0.35

can occur at a relative lower temperature.[13,38] Moreover, from Figure 2, with a constant cooling rate, the T_p increased with addition of mica particles into PBS matrix, and it exhibited apparent dependence on the content of mica. Liang et al. found a similar increasing phenomenon during the non-isothermal process for the PBS/functional multi-walled carbon nanotube Nano composites with DSC method.[12] It seemed that the mica particles had a significant heterogeneous nucleation effect on the non-isothermal crystallization process for PBS matrix.

Crystallization Rate Coefficient. In order to get a straightforward compare about the rate of crystallization rate for pure PBS and its composites during non-isothermal crystallization process, the parameter titled "crystallization rate coefficient (CRC)" was employed by Khanna.[36] The CRC values can be obtained from the slopes of the curves about the cooling rates φ versus the crystallization peak temperatures T_p and it showed a variation in cooling rate which is needed to result in 1°C change in the supercooling for the polymer.[36] Therefore, we could infer the conclusion that the higher CRC values imply the crystallization rate is faster. Figure 3 showed the curves of cooling rate φ versus T_p. The values of CRC are 89.5, 102.2, 109.1, 120.3, and 121.3 h^{-1} for neat PBS, mica/PBS (1/99), mica/PBS (2/98), mica/PBS (4/96), and mica/PBS (8/92) samples during the non-isothermal process, respectively, leading to the conclusion that the rate of crystallization for mica/PBS composites increased with the increase of mica content.

Non-isothermal Crystallization Kinetics

In this study, the non-isothermal crystallization process was further researched by comparing the non-isothermal crystallization

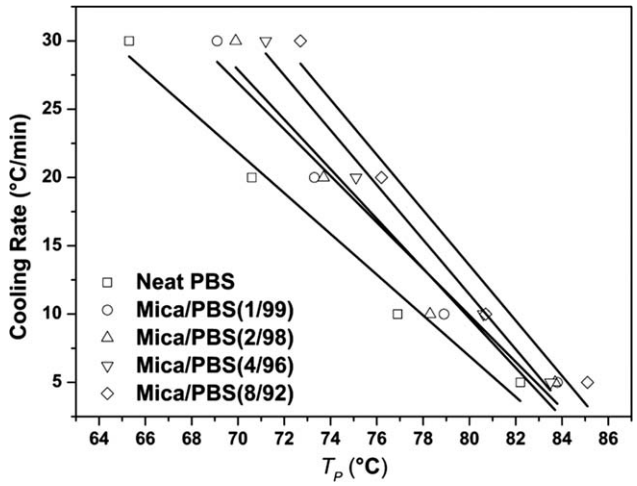

Figure 3. Plots of cooling rate versus the crystallization peak temperature T_p based on Khanna's treatment.

kinetics of pure PBS and its composites. From the DSC curves obtained during the crystallization, the values of relative crystallinity (X_t) at constant cooling rates which is a function of temperature could be obtained from the below *eq.* (1):

$$X_t = \frac{\int_{T_0}^{T} (dH_c/dT)dT}{\int_{T_0}^{T_\infty} (dH_c/dT)dT} \quad (1)$$

where H_c is the enthalpy for the crystallization, T_0 is the onset temperature, and T_∞ is the end temperature for the crystallization process, dH_c/dT represents the heat flow rate. Generally, the temperature T for the crystallization can be changed into the time t for the crystallization in the following equation:

$$t = \frac{T_0 - T}{\varphi} \quad (2)$$

where φ represents the rate about temperature change for the cooling process, T stands for the specific crystallization temperature at the corresponding crystallization time t. Base on *eqs.* (1) and (2), Figures 4 and 5 presented the relative crystallinity versus the crystallization temperature T and the relative crystallinity versus crystallization time t for neat PBS and mica/PBS (4/96) composite at several different constant cooling rates φ, respectively.

From Figure 4, an obvious sigmoid was shown in all the curves, predicting a thermal lag effect from different constant cooling rate during the crystallization process.[38] That is, with a lower cooling rate crystallization happened at the higher temperature. And with a higher cooling rate crystallization happened at the lower temperature. Generally speaking, as the rate of cooling is low, the time for the nucleation process at the high temperature is enough.

It was shown from Figure 5 that the all the shapes were very similar. Also, it can be observed that the sigmoidal curves shift to shorter time when the cooling rate increases, leading to the conclusion that the time for the whole crystallization process is relative shorter with the increase of the cooling rate.

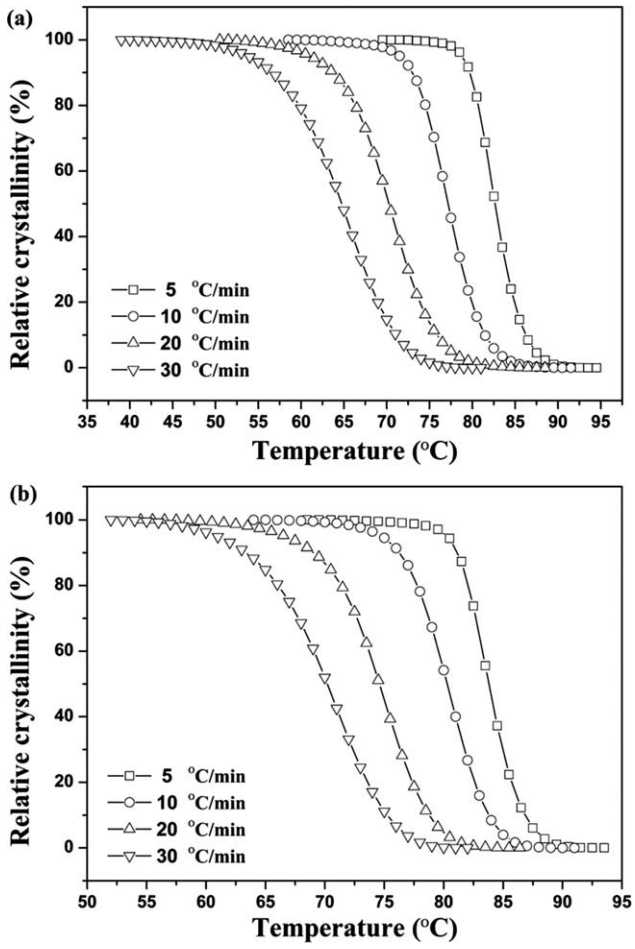

Figure 4. Development of relative crystallinity (X_t) versus temperature (T) for non-isothermal melts crystallization of (a) neat PBS and (b) mica/PBS (4/96) composite at different cooling rates.

Furthermore, the curves of mica/PBS composites shifted toward shorter crystallization time with a constant cooling rate, demonstrating that the crystallization rate of mica/PBS composites during the non-isothermal crystallization process is higher than the crystallization rate of neat PBS.

Additionally, from the figures and dates above, a significant factor was the half-time for the crystallization process ($t_{1/2}$), obtained by using the next equation:

$$t_{1/2} = \frac{T_0 - T_{1/2}}{\varphi} \quad (3)$$

where $T_{1/2}$ is the crystallization temperature during the crystallization process when the relative crystallinity is 50%. The half crystallization times ($t_{1/2}$) obtained from Figure 5 were listed in Table I. It was apparent that the $t_{1/2}$ value became lower when the cooling rate increased, indicating that crystallization rates for pure PBS and mica/PBS composites were higher when the cooling rate was increased. Furthermore, all the $t_{1/2}$ values of mica/PBS composites were lower than the $t_{1/2}$ values for pure PBS with a constant cooling rate, showing that the crystallization rate for the non-isothermal crystallization process was higher with the addition of mica particles. Some researchers had also found the similar results in PBS/Silica nanocomposites.[6] The

Applied Polymer SCIENCE

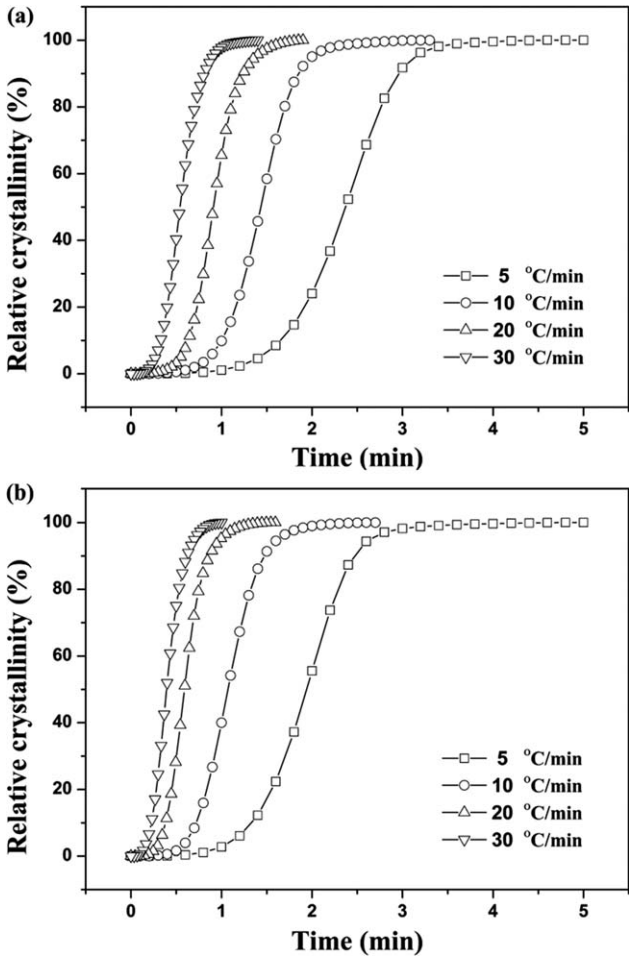

Figure 5. Development of relative crystallinity (X_t) versus time (t) for non-isothermal melts crystallization of (a) neat PBS and (b) mica/PBS (4/96) composite at different cooling rates.

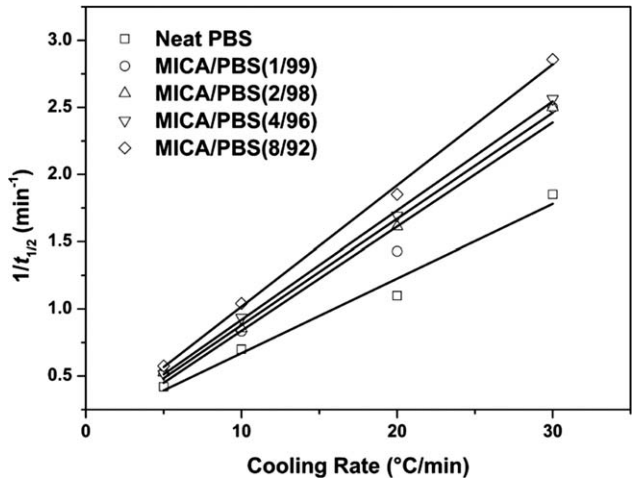

Figure 6. Plots of $1/t_{1/2}$ versus the cooling rate for neat PBS and its composites with different mica contents.

reason for the increase of the crystallization rate may be that the mica particles take an obvious heterogeneous nucleation effect.

The other important factor titled crystallization rate parameter (CRP) was employed here for the research on the non-isothermal crystallization rate. The CRP values can be obtained from the slopes of a curve about $1/t_{1/2}$ versus cooling rate.[39,40] The higher the slope is, the faster the crystallization rate is. Figure 6 presented the curves of $1/t_{1/2}$ versus the cooling rate. The CRP values were 0.05556, 0.07757, 0.07908, 0.08128, and 0.09018 for pure PBS, mica/PBS (1/99), mica/PBS (2/98), mica/PBS (4/96), and mica/PBS (8/92) samples, respectively, implying crystallization rate was increased when mica particles were added into PBS matrix. Furthermore, the CRP values were increased when the loading level of mica particles were increased. It appeared that mica particles took an obvious heterogeneous nucleation effect promoting the crystallization for the non-isothermal process. Similar phenomenon had also been reported in PBSU/f-MWNTs composites by Liang Song and Zhaobin Qiu.[12] They reported that the crystallization of PBS would be promoted by the higher functional multi-walled carbon nanotubes content and this result was caused by the significant heterogeneous nucleation of f-MWNTs on the crystallization and morphology of PBS.

In order to better investigate the non-isothermal crystallization behavior of pure PBS and its composites, three methods were used here to study the non-isothermal crystallization kinetics, including Avrami model, Ozawa model, and combined Avrami–Ozawa model.

Avrami Model

Avrami model is a widely used theory to study the crystallization kinetics.[41,42] For the isothermal crystallization condition the Avrami equation was usually employed. Moreover, the Avrami equation can be also employed for the non-isothermal crystallization process. The Avrami equation can be expressed as following:

$$1-X_t=\exp\left(-Z_t t^n\right) \tag{4}$$

where n denotes the Avrami exponent determined by the type of nucleation and growth, X_t is relative crystallinity, and Z_t represents the crystallization rate constant involving growth rate and nucleation. Then the double logarithmic type of the equation above could be deduced as following:

$$\log\left[-\ln(1-X_t)\right]=n\log t+\log Z_t \tag{5}$$

Thus, with different cooling rates, the Avrami curves of log $[-\ln(1 - X_t)]$ as a function of log(t) for neat PBS and mica/PBS composites were plotted in Figure 7, and the intercepts and slopes of the Avrami curves denote the values for rate parameter Z_t and Avrami exponent n, respectively. And, these two values were listed in Table II. However, the physical significance of n and Z_t for non-isothermal crystallization process is different with the meaning for isothermal crystallization process for the reason that the constant change in temperature influences both the nuclei formation and the growth of spherulite. Thus, these values of n and Z_t for the non-isothermal crystallization should be corrected, and a lot of scientists had done much work for

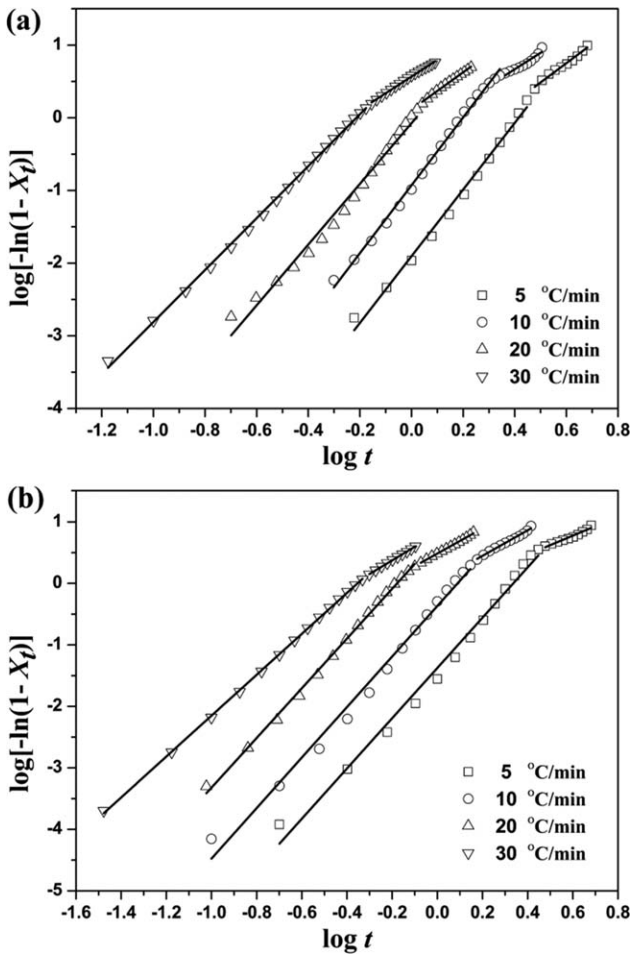

Figure 7. Avrami plots of $\log[-\ln(1 - X_t)]$ versus $\log t$ for non-isothermal melt crystallization of (a) neat PBS and (b) mica/PBS (4/96) composite.

the correction of Avrami equation with the physical truth.[36,38] Considering the constant change in temperature and the cooling rate (φ), Jeziorny[43] fully changed Z_t as following equation:

$$\log Z_c = \frac{\log Z_t}{\phi} \tag{6}$$

where Z_c denotes the crystallization rate constant. And, the Z_c values were shown in Table II.

In Figure 7, we can separate the curves for pure PBS and its composites into two parts. These two parts are the secondary crystallization and the primary crystallization.[38] With all cooling rates in each section the plots for matching the curves were almost in the same shape. Thus, it can be concluded that the mechanism about the formation of nucleation and growth of crystal for a special sample were similar regardless of changing the cooling rate.

In Table II, the Avrami exponent n_1 for the primary crystallization of pure PBS were larger than that of its composites, suggesting that it was complex to the composites in the formation of nucleation and growth of crystal. For mica/PBS composites, those mica particles play a role as heterogeneous nucleation, leading to an obvious mechanism of heterogeneous nucleation to non-isothermal crystallization process. The Avrami exponent n_2 for the secondary crystallization denotes about 2.0. Thus, it can be concluded that the growth of crystal denotes a two-dimensional mode. On the other hand, at the same φ, the Z_c values of mica/PBS composites were higher than that of neat PBS, indicating crystallization rates of the composites were larger than pure PBS's. Moreover, the Z_c values which were shown in Table II increased for both pure PBS and its composites when the cooling rate increased, indicating that PBS could crystallize in a shorter time when cooling rate was increased. This was caused by the fact that when cooling rate is larger, crystallization would take place with a lower temperature and the crystallization rate of PBS is bigger for the reason that the undercooling is larger.

Ozawa Model

Based on Avrami equation (4), Ozawa[44] have considered φ's role for the non-isothermal crystallization, replaced time t in *eq.* (4) with T/φ, and modified the Avrami equation. It is supposed that the crystallization is processed with an unaltered φ (cooling rate). Based on Ozawa's theory, the relationship between X_t at T and the cooling rate (φ) can be obtained as following:

$$1 - X_t = \exp[-K(T)/\phi^m] \tag{7}$$

where $K(T)$ denotes the cooling crystallization function, m represents the Ozawa exponent depending on the growth of crystal geometry, and process of nucleation, X_t denotes the relative degree of crystallinity, and φ denotes the cooling rate for the non-isothermal crystallization. In this case, analysis can be obtained for a fixed temperature T using the transformation of *eq.* (7) in the double-logarithmic form as follow:

$$\log[-\ln(1 - X_t)] = \log K(T) - m\log\phi \tag{8}$$

According to the equation above, on condition that the curve of $\log[-\ln(1 - X_t)]$ as a function of $\ln\varphi$ is approximately a line for a specific temperature, the Ozawa equation could represent non-isothermal crystallization kinetics for pure PBS and its composites, and the Ozawa exponent m and the kinetic parameters $K(T)$ could be estimated by the slope and the intercept of the line, respectively. It is widely used in many polymers for Ozawa equation during non-isothermal crystallization.[35] The curves of Ozawa model as $\log[-\ln(1 - X_t)]$ versus $\log\varphi$ for neat PBS and mica/PBS (4/96) composite are shown in Figure 8. Although some plots showed approximate linearity from Figure 8, the deviation of the plots from the straight line were also observed, implying that for neat PBS and mica/PBS composites appropriate study cannot be achieved by using Ozawa method for non-isothermal crystallization. This result is because of that to Ozawa model the secondary crystallization process observed in this study is usually neglected and Ozawa exponent m is thought to be stable from beginning to the end of the process. Similarly, other researchers had also reported that the non-isothermal crystallization process of PBS and its composites cannot

Table II. Non-isothermal Crystallization Kinetic Parameters Based on Avrami and Jeziorny Model

		Primary crystallization			Secondary crystallization		
Sample	φ (°C/min)	n_1	log Z_{t1}	Z_{c1}	n_2	log Z_{t2}	Z_{c2}
PBS	5	4.403	−1.851	0.426	2.653	−0.839	0.679
	10	4.621	−0.931	0.807	2.446	−0.322	0.929
	20	4.177	−0.074	0.992	2.564	0.114	1.013
	30	3.491	0.728	1.058	2.295	0.568	1.045
Mica/PBS (1/99)	5	4.585	−1.442	0.515	2.052	−0.381	0.839
	10	4.150	−0.895	0.814	1.735	−0.278	0.938
	20	3.897	0.365	1.043	2.041	0.364	1.043
	30	3.377	1.137	1.091	1.767	0.723	1.057
Mica/PBS (2/98)	5	4.379	−1.388	0.528	1.794	−0.265	0.885
	10	3.777	−0.526	0.886	1.955	0.016	1.004
	20	3.617	0.560	1.067	1.957	0.446	1.053
	30	3.436	1.202	1.097	1.970	0.728	1.057
Mica/PBS (4/96)	5	4.089	−1.375	0.531	1.542	−0.149	0.934
	10	4.110	−0.367	0.919	2.076	0.034	1.008
	20	4.044	0.721	1.087	2.048	0.486	1.058
	30	3.391	1.211	1.097	2.213	0.816	1.065
Mica/PBS (8/92)	5	4.348	−1.271	0.557	1.697	−0.119	0.947
	10	3.881	−0.202	0.955	2.342	0.080	1.019
	20	3.713	0.789	1.095	1.979	0.516	1.061
	30	3.199	1.296	1.105	2.015	0.826	1.065

be studied by the Ozawa theory due to their obvious secondary crystallization.[13,39]

Liu Model (Combined Avrami–Ozawa Model)

As stated above, the non-isothermal crystallization process for neat PBS and mica/PBS composites cannot be studied by the Ozawa theory. Because X_t which is the degree of crystallinity is influenced by the crystallization time t and the cooling rate (φ) from the Avrami and the Ozawa model, respectively. Liu et al.[45] proposed an effective method to study the non-isothermal crystallization kinetics by using the modification of the Ozawa model and the Avrami method as follows:

$$\log Z_t + n \log t = \log K(T) - m \log \phi \tag{9}$$

In *eq.* (9), the left side of the equation above is from the Avrami method, the right side of the equation above is from the Ozawa equation, n denotes the Avrami exponent and m denotes Ozawa exponent. Both the two exponents are depending on the formation of nuclei and the growth of spherulite. At a given degree of crystallinity X_t, the equation above can be rearranged into the following equation:

$$\log \phi = \log F(T) - \alpha \log t \tag{10}$$

where α is the quotient of the Avrami exponent n divided by the Ozawa exponent m. The factor $F(T) = [K(T)/Z_t]^{1/m}$ is contacted with the quantitative value of φ which is required in a unit interval during crystallization when the systems have obtained a certain X_t. Thus, the parameter $F(T)$ is full of appropriate practical significance for the crystallization kinetics. It can be indicated that when the $F(T)$ value is larger, the needed φ value is also larger for obtaining a certain X_t in a unit interval.

Based on *eq.* (10), the curve of log φ as a function of log t at a specific X_t should be linear and the kinetic factor $F(T)$ and a for non-isothermal crystallization could be estimated by the intercept and slope of the curve, respectively.

In Figure 9, it can be seen that obvious linearity is shown in the curves. Thus, the combined Avrami–Ozawa method is good in studying the kinetics of non-isothermal crystallization for pure PBS and mica/PBS composites. The values for kinetic a and parameter $F(T)$ determined from the slope and the intercept of the curves at a special X_t were shown in Table III. We can see that with a specific mica loading the a value increased when the X_t value increased and at a specific X_t the a values for neat PBS are larger than that for mica/PBS composites. The $F(T)$ value systematically increased when X_t value increased, showing that a larger cooling rate was needed to realize a larger X_t value in a unit interval. At the same relative crystallinity X_t, the $F(T)$ values for pure PBS was larger than mica/PBS composites', indicating the crystallization rate of mica/PBS composites was larger than pure PBS's. Also, it can be concluded that the crystallization rate during non-isothermal crystallization was increased by the mica particles. In addition, the $F(T)$ values was reduced when the loading of mica particles was increased, showing the larger content of mica particles, the higher the

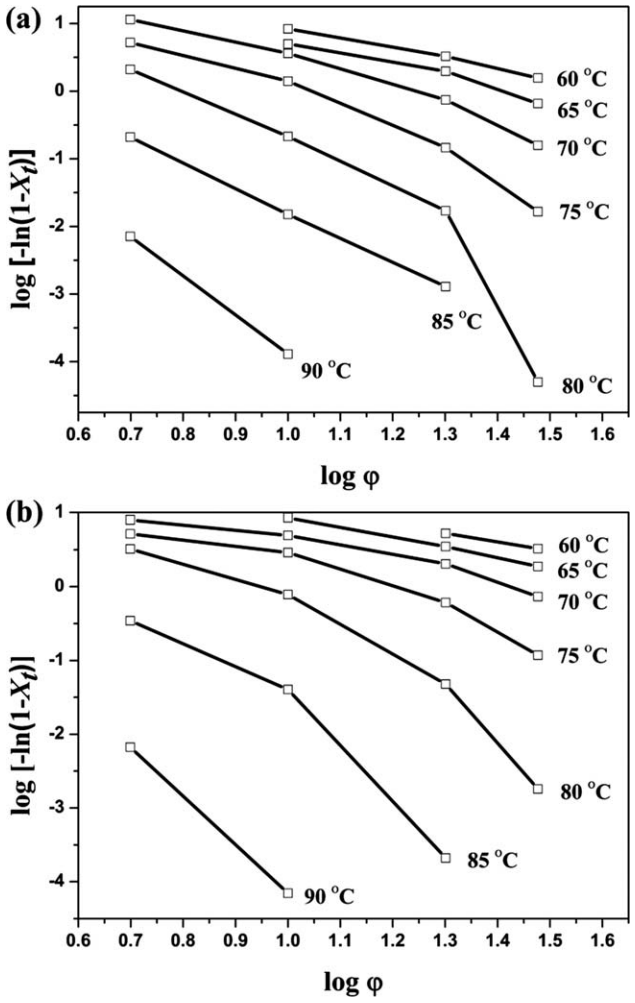

Figure 8. Ozowa plots of log[$-\ln(1 - X_t)$] versus log φ for non-isothermal melt crystallization of (a) neat PBS and (b) mica/PBS (4/96) composite.

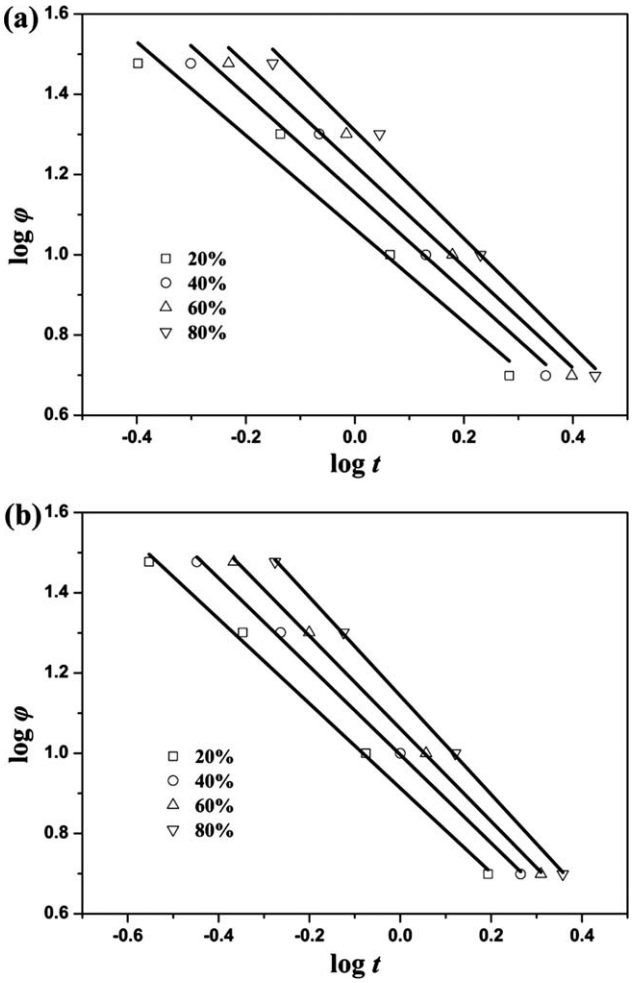

Figure 9. Plots of log φ versus log t for non-isothermal melt crystallization of (a) neat PBS and (b) mica/PBS (4/96) composite.

crystallization rate. Hence, mica particles might act as a role of heterogeneous nucleation and induce a typical heterogeneous nucleation mechanism. We can see that the study from the combined Avrami–Ozawa method is similar with the result above from the Avrami model. Also, in the next part of this article, we verify the heterogeneous nucleation effect of mica particles to PBS matrix by the polarizing microscope.

Clearly, with the advantage of correlating the φ (cooling rate) to the other important factors including the crystallization time t, the formation of nucleation, the growth of crystal, the crystallization temperature T, the kinetics of non-isothermal crystallization kinetics for neat PBS, and mica/PBS composites can be good investigated by the modified Avrami–Ozawa method. By using the modified Avrami–Ozawa method many researchers had studied properly in a lot of polymeric and polymer composite systems.[38]

Spherulitic Morphology and Crystalline Structure

The spherulitic morphology was studied by using the polarizing microscope for pure PBS and its composites. In Figure 10, we can see the polarized micrographs for pure PBS and its composites. From Figure 10(a), we can see that the big spherulites and Maltese cross were very obvious for pure PBS. Also, in Figure 10(b), we can see apparently with the presence of mica particles the density value of the nucleation was raised and the size value of the spherulite was reduced, indicative of stronger heterogeneous nucleation effect of mica. Therefore, we can conclude that by the nucleating effect of mica particles the density value of the nucleation was raised, the shape of the spherulite was made irregular, and the size value of the spherulite was reduced.[39] However, this result emphasizes the enhancement of nucleation with the addition of mica particles. From the study of polarizing microscope for pure PBS and mica/PBS composites, we can indicate that the nucleation effect of mica particles plays more important role in the non-isothermal crystallization of mica/PBS composites, leading to the result that the crystallization rate was raised for PBS matrix during non-isothermal crystallization despite of the mica's defects of more constraints on the growth of crystal. Furthermore, this result was fitted with the study above from the Avrami model and the combined Avrami–Ozawa method on the DSC analysis in the previous section.

It was also necessary to investigate the influence of the mica particles for PBS matrix on the crystal structure before and after

Table III. Non-isothermal Crystallization Kinetic Parameters Based on Liu Model

X_t(%)		20	40	60	80
PBS	α	1.163	1.221	1.264	1.345
	$F(T)$	11.613	14.259	16.729	20.396
Mica/PBS (1/99)	α	1.098	1.139	1.18	1.256
	$F(T)$	8.795	10.698	12.502	14.973
Mica/PBS (2/98)	α	1.06	1.113	1.164	1.25
	$F(T)$	8.424	10.29	12.079	14.576
Mica/PBS (4/96)	α	1.054	1.101	1.155	1.23
	$F(T)$	8.188	9.918	11.517	13.906
Mica/PBS (8/92)	α	1.03	1.103	1.175	1.271
	$F(T)$	7.361	8.815	10.224	12.378

composite preparation. In Figure 11, by using the wide-angle X-ray diffraction (WAXD) analysis we study the crystalline structure of pure PBS and its composites. The pure mica shows five distinct reflection peaks around 2θ = 9.5°, 19.0°, 28.7°, 29.5°, and 31.0°. Also, we can see that for pure PBS several strong diffraction peaks at 2θ values of 28.9°, 22.6°, and 19.6° was displayed, in accordance with (1 1 1), (1 1 0), and (0 2 0) planes, respectively.[13] Therefore, for mica/PBS composites, the shifts of diffraction peaks in position with mica content are not observed, indicating that the mica particles did not modify the crystalline structure of PBS. Moreover, the increasing addition of mica Particles make the diffraction peaks' intensity reduced.

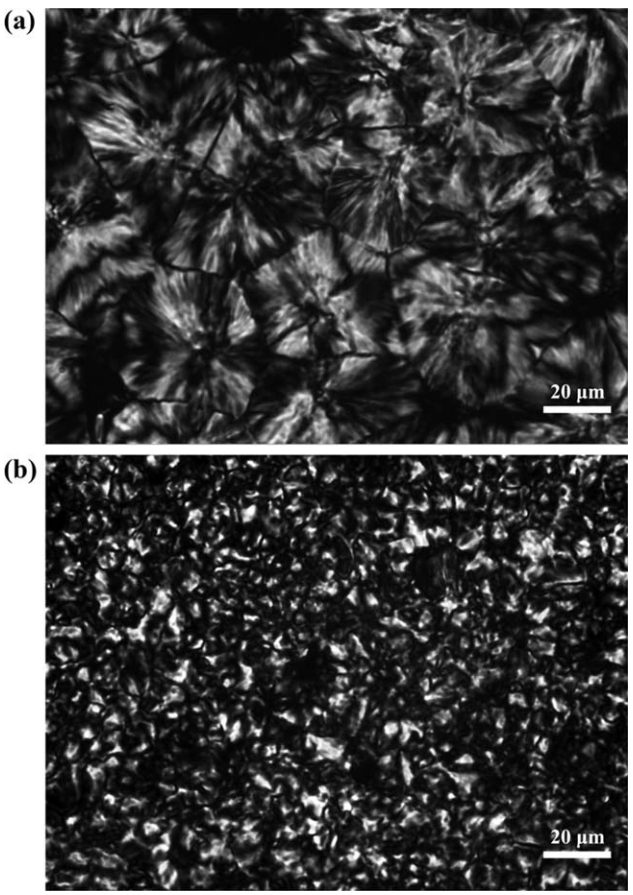

Figure 10. Optical micrographs of (a) neat PBS and (b) mica/PBS (4/96) composite (both non-isothermally crystallized).

Activation Energy of Crystallization for the Non-isothermal Processes

The widely use of DSC equipment make the crystallization kinetics properly studied by the Avrami equation (4). According to the *eq.* (4), a lot of researchers have made the Avrami Equation properly used in the non-isothermal crystallization process. In Avrami Equation, the value of Z_t usually can be obtained by the use of the Arrhenius equation as following,

$$Z_t = A \times \exp\left(-\frac{E}{RT}\right) \tag{11}$$

where E denotes the activation energy, R denotes the gas constant, T represents the thermodynamic temperature, A represents the factor of pre-exponent. In particular, from the Arrhenius equation, E could be calculated for non-isothermal

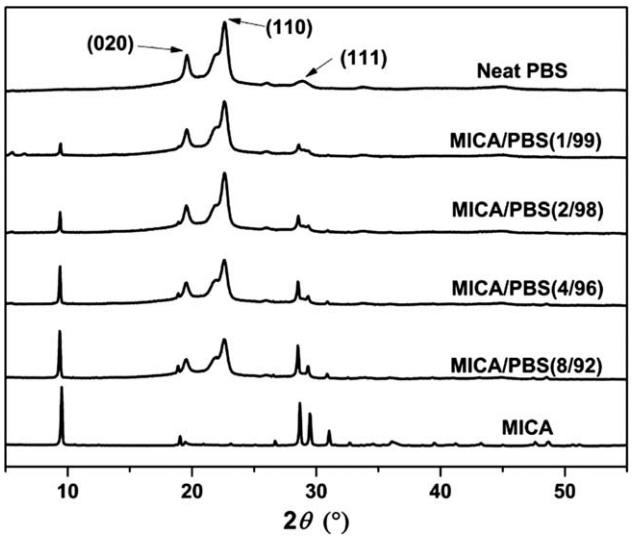

Figure 11. WAXD patterns of neat PBS, mica, and mica/PBS composites.

crystallization by combining the peak temperature T_p and φ in the following models[14]:

Kissinger model:

$$\frac{d[\ln(\phi/T_p^2)]}{d(1/T_p)} = -\frac{E}{R} \tag{12}$$

Takhor model:

$$\frac{d[\ln(\phi)]}{d(1/T_p)} = -\frac{E}{R} \tag{13}$$

Augis–Bennett model:

$$\frac{d\{\ln[\phi/(T_0 - T_p)]\}}{d(1/T_p)} = -\frac{E}{R} \tag{14}$$

According to the three equations above, the E values of pure PBS and its composites for non-isothermal crystallization can be got by using the slope of the curves about $\ln(\phi/T_p^2)$ versus $1/T_p$, $\ln(\phi)$ versus $1/T_p$, and $\ln[\phi/(T_0 - T_p)]$ versus $1/T_p$, respectively. Both Bian and Chen had used the Kissinger model to determine the crystallization activation energies for poly(butylene succinate) composites, respectively.[6] By using the Takhor model, Yang and Wu had calculated the crystallization activation energies for poly(ε-caprolactone)/layered double hydroxide nano-composites and polyamide 11 composites, respectively.[38,39] Moreover, Ohkita had used all the three models above to calculate the crystallization activation energies for poly(butylene succinate)/corn starch biodegradable composite.[14]

However, some experts have recently demonstrated[46] that these methods cannot study the activation energy very well when the polymer or polymer composites are processed under cooling. Moreover, these three models were restricted in the calculation of the activation energy as they can only provide a single value of the activation energy for the crystallization process.[47] For these reasons the very popular theory Hoffman–Lauritzen theory was used in here to study the activation energy of pure PBS and its composites for the non-isothermal crystallization process.[48]

The Hoffman and Lauritzen[48] theory is very popular in studying the growth of crystal which occurs during the isothermal crystallization process. Several experts have also used the Hoffman and Lauritzen[48] theory properly for the non-isothermal crystallization.[46,48] On the basis of the Hoffman–Lauritzen theory, G, the rate of spherulitic growth is influenced by two important factors, including the cooling rate φ and the temperature T. Thus, G was displaced in the following equation from the Hoffman–Lauritzen theory:

$$G = G_0 \exp\left(-\frac{U^*}{R(T - T_\infty)}\right) \exp\left(-\frac{K_g}{T(\Delta T)f}\right) \tag{15}$$

where G_0 represents the parameter of pre-exponent that is independent from the crystallization process. The right exponential factor is $\exp\left(-K_g/T(\Delta T)f\right)$ which is influenced by the formation of the nucleation. The left exponential factor is $\exp(-U^*/R(T - T_\infty))$ which is influenced by the growth of crystal. In the left exponential factor of the equation above, R which influences the growth of crystal denotes the universal gas constant, U^* which is generally taken to be the constant value as 1500 cal/mol represents the activation energy for the growth of crystal including the transportation of the chains during non-isothermal process. T_∞ whose temperature value is lower than T_g (the temperature of the glass transition) by 30° means that at such temperature all flows of the polymer system stop flowing. In the right exponential factor of the equation above K_g which is influenced by the degree of undercooling denotes the activation energy for the formation of nucleation, DT which are calculated from the difference between the T_m^0 minus T denotes the degree of undercooling, T_m^0 denotes the equilibrium melting temperature, and f which equals the quotient of $2T$ divided by $(T_m^0 + T)$ represents the correction factor. Moreover, the nucleation parameter K_g is obtained using the equation as following:

$$K_g = \frac{nb_0\sigma\sigma_e T_m^0}{\Delta h_f k_B} \tag{16}$$

where b_0 denotes the crystal layer thickness which is along the growth direction, σ_e denotes the free energy of the fold surface, σ represents the free energy of the lateral surface, k_B represents the Boltzmann constant, Δh_f denotes the heat of fusion for the unit volume in crystal. Furthermore, the value of n was influenced by the type of crystallization regime. When the type of crystallization regime is I and III, the value of n denotes 4. When the type of crystallization regime is II, the value of n denotes 2.

A lot of researchers have used the Hoffman–Lauritzen theory to confirm the value of E activation energy for the non-isothermal and isothermal crystallization in a variety of ways.[49] There are two kinds of methods for the calculation of E activation energy. One type is the advanced isoconversional method which is the method of Vyazovkin et al., the other type is the differential isoconversional methods, including the methods of Ozawa, the model of Friedman, the method of Flynn and Wall, and so on.[46,47,49] We took the Friedman model for the E activation energy of pure PBS and its composites during non-isothermal crystallization. On the basis of the Friedman model, energy E in different degree of crystallinity is calculated from[49]:

$$\ln\left(\frac{dX}{dt}\right)_{X,\phi} = \text{Const} - \frac{E_X}{RT_{X,\phi}} \tag{17}$$

Here, dX/dt denotes the derivative of the relative degree of crystallization X_t on the crystallization time t, φ denotes the specific cooling rate for the non-isothermal crystallization process, $T_{X,\phi}$ denotes the specific crystallization temperature T for a specific cooling rate φ and a specific relative degree of crystallization X_t, E_X denotes the activation energy for a specific relative degree of crystallization X_t. On the basis of the model

proposed by Vyazovkin,[47,49] the calculation of E_X based on the crystallization rate, the cooling rate, the crystallization time, and the crystallization temperature can be derived from *eqs.* (15) and (17):

$$E_X(T) = -R\frac{d\ln(dX/dt)}{dT^{-1}} = -R\frac{d\ln G}{dT^{-1}} = U^*\frac{T^2}{(T-T_\infty)^2} + K_g R\frac{(T_m^0)^2 - T^2 - T_m^0 T}{(T_m^0 - T)^2 T} \quad (18)$$

where $E_X(T)$ denotes the activation energy of pure PBS and its composites with a specific relative degree of crystallization X_t, the subscript X is the relative degree of crystallization at the crystallization temperature T. Because of the change in the cooling rate φ, the equal degree of crystallization X can be accomplished by the different crystallization temperatures T. Thus, we can get a mean temperature of the different crystallization temperatures T for a specific relative degree of crystallization X_t, and the effective activation energy $E_X(T)$is calculated on the basis of mean temperature needed for the *eq.* (17).

Figure 12 displays the active energy $E_X(T)$ versus the mean temperature of the different crystallization temperatures T according to the different cooling rate φ at the same relative degree of crystallization X_t. It is clear that the $E_X(T)$ values are less than zero, implying for pure PBS and its composites the non-isothermal crystallization is an exothermic process. Therefore, the absolute value of $E_X(T)$ is adopted to study the active energy for the non-isothermal crystallization process. Also, it can be concluded that when the value of $|E_X(T)|$ is larger, more energy is needed for the non-isothermal crystallization process. Thus the higher $|E_X(T)|$ value exhibits the lower crystallization ability. From Figure 12, we can also see that the crystallization rate is decreased when the temperature is increased for pure PBS and its composites. Moreover, the $|E_X(T)|$ value of pure PBS was larger than the value of its composites, indicating that it was easier for PBS to crystallize when the mica particles were blended with the PBS matrix. Therefore, we can conclude that there is a heterogeneous nucleation effect caused by the addition of mica particles. Additionally, this result is in accordance with the results from Avrami and Liu model mentioned above.

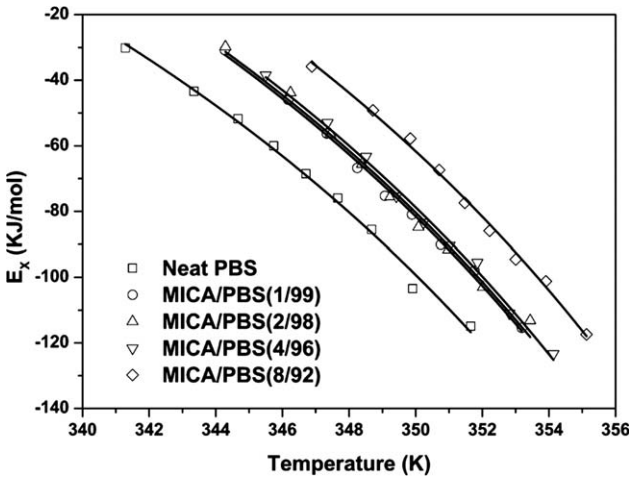

Figure 12. Dependence of the effective active energy on average temperature for neat PBS and mica/PBS composites. Solid lines represent fits of *eq.* (18).

According to our data in Figure 12, we could evaluate K_g and $U^\star$ which are titled the Hoffman–Lauritzen Parameters by matching *eq.* (18) with the dependence of $E_X(T)$ on crystallization temperature T. From the *eq.* (18) it is very important to confirm T_g (the glass-transition point) and T_m^0 (the equilibrium melting point) before the calculation of the Hoffman–Lauritzen parameters. In this investigation, the values of T_g and T_m^0 denote 243 K and 399 K respectively, according to Hwang's research.[50] For confirming the values of the Hoffman–Lauritzen parameters (U^* and K_g), we used the model of the Levenberg–Marquardt to fit the plots with a fitted non-linear curve. It is noteworthy in Figure 12 that the theoretical results are obviously suitable for the experiment dates. The Hoffman–Lauritzen parameters calculated from the non-linear curve were listed in Table IV.

In addition, the values of $\sigma\sigma_e$ (the free energy of the surface) were obtained by using the confirmed values of K_g (the activation energy of the nucleation) according to *eq.* (16). For the calculation of the surface free energy $\sigma\sigma_e$, b_0 which is the thickness value of the monomolecular layer are 0.404 nm because of the α-form unit cell of PBS which are determined in Figure 11.[13] The value of n is chosen to be 2 because the type of crystallization regime is II.[51] The value of Δh_f which is the bulk melting enthalpy in a unit volume determined as the mass heat of fusion times the density is selected to be 146.70×10^6 J/m^3.[35] According to the factors chosen above, the surface free energy $\sigma\sigma_e$ was calculated on the basis of *eq.* (16).

Finally, the evaluated values of $U^\star$, K_g, and $\sigma\sigma_e$ were shown in Table IV. According to $K_g = 0.84 \times 10^5$ K^2 studied by Hwang et al., 0.80×10^5 K^2 calculated by Soccio et al., and 0.745×10^5 K^2 calculated by Park et al.,[50,52,53] respectively, the Hoffman–Lauritzen parameters K_g was 1.86×10^5 K^2 in this study which appeared to be larger than the reported values. The larger value of K_g in this study was caused by the reason that from *eq.* (18) the Hoffman–Lauritzen parameters $U^\star$ and K_g were fitted, but the reported values were calculated on the basis of the stable $U^\star$ value as 6300 J/mol.[13] However, in this case, it was statistically unacceptable to use the universal value of $U^\star$ for the reason that it was very proper to fit both K_g and $U^\star$ from *eq.* (18). In addition, it was also reported that the Hoffman–Lauritzen parameters $U^\star$ which usually was treated as a universal

Table IV. Hoffman–Lauritzen Parameters of Neat PBS and mica/PBS Composites

Sample	$K_g \times 10^{-5}$ (K^2)	U^* (KJ/mol)	$\sigma\sigma_e \times 10^4$ (J^2/m^4)
Neat PBS	1.86	13.94	11.69
Mica/PBS (1/99)	1.83	16.01	11.50
Mica/PBS (2/98)	1.82	16.09	11.43
Mica/PBS (4/96)	1.81	16.22	11.37
Mica/PBS (8/92)	1.70	17.08	10.68

value 6300 J/mol was usually in the range of 4.2 to 16.7 kJ/mol in the experiment studied by Hoffman et al.[47] By using the experiment data in this research, the Hoffman–Lauritzen parameters U^* from the fitting line is 13.94 kJ/mol. Obviously the Hoffman–Lauritzen parameters U^* was higher than the universal value. The Hoffman–Lauritzen parameters U^* and K_g and the surface free energy $\sigma\sigma_e$ in this study were obviously larger. This result is in accordance with the research findings that the larger value of U^* resulted in obtaining a larger K_g which are reported by Hoffman et al. and Vyazovkin et al.[46,47,49]

Moreover, in Table IV, it was displayed that the U^* values were enhanced, but the K_g values and $\sigma\sigma_e$ values were reduced with the increased loading of mica particles, indicating that mica particles played a dual role in the non-isothermal crystallization process involving the formation of the nucleation and the growth of crystal. On one hand, the nucleation processes of mica/PBS composites were accelerated as the mica particles were added into PBS matrix. The interfacial free energy was lessened and the non-isothermal crystallization rate of the mica/PBS composites was accelerated by the mica particles. Therefore, the mica particles played a role as agents of nucleation reducing the activation energy for the nucleation process, leading to a lower K_g and $\sigma\sigma_e$. On the other hand, when the mica particles were blended with the pure PBS, the mobility of PBS chains decreased, and the PBS chains should conquer larger energy barriers for the growth of crystal during the non-isothermal crystallization. The presence of mica particles played a role as impediments to retard the mobility of PBS chains and hinder the growth of crystal by inducing restriction on the PBS chains, leading to a larger U^*. However, these two competing roles are in contradiction with each other on the PBS's crystallization. Furthermore, from the results of the Avrami method and combined Avrami–Ozawa method, we can see the mica's nucleating effect is prevailing over the retarding effect to PBS matrix. The crystallization rate of the composites was larger than the pure PBS's.

CONCLUSIONS

The crystallization behavior of pure PBS and its composites with mica particles were studied in this research. Both the values of CRC and CRP increased when the content of mica particles were increased, suggesting the mica particles played a role as nucleation agents. On the basis of the Avrami approach, Ozawa method and the combined Avrami–Ozawa equation, the kinetics for the crystallization process was studied. As a result, the Ozawa model did not well match the experimental dates, while the Avrami analysis and the modified Avrami–Ozawa method satisfactorily studied the crystallization of these systems, showing that the crystallization rate of PBS was enhanced by the mica particles.

The addition of mica particles played a role as nucleation agents to induce more nuclei, reduce the size of spherulite, and make the shape of the spherulite irregular. And, the crystalline structure of PBS was not modified by the incorporation of mica particles into the PBS matrix.

The activation energy of the pure PBS was larger than the composites with mica particles. The analysis showed that mica particles played two different roles to the PBS matrix: the mica particles played a role as agents for the formation of nucleation to promote the crystallization, while they played the other role as impediments to retard the growth of crystal. The former was dominating as the crystallization rate of mica/PBS composites was accelerated.

ACKNOWLEDGMENTS

We thank the National Nature Science Foundation of China (Grant 10872071, 50973035 and 50903033), the Fundamental Research Funds for the Central Universities (NO.2011ZM0063), the National Key Technology R&D Program of China (Grant 2009BAI84B05 and 2009BAI84B06), the Program for Changjiang Scholars and Innovative Research Team in University (IRT0827), and the National Natural Science Foundation of China-Guangdong Joint Foundation Project (U1201242) for their fund.

REFERENCES

1. Li, H.; Chang, J.; Cao, A.; Wang, J. *Macromol. Biosci.* **2005**, *5*, 433.
2. Vroman, I.; Tighzert, L. *Materials* **2009**, *2*, 307.
3. Rhee, S. H.; Lee, Y. K.; Lim, B. S. *Biomacromolecules* **2004**, *5*, 1575.
4. Ray, S. S.; Bousmina, M. *Macromol. Chem. Phys.* **2006**, *207*, 1207.
5. Hiromi, U.; Toshiaki, N. K.; Yukie, S. A.; Nobuhiko, N.; Yutaka, T.; Tadaatsu, N. *FEMS Microbiol. Lett.* **2000**, *189*, 25.
6. Bian, J.; Han, L.; Wang, X.; Wen, X.; Han, C.; Wang, S.; Dong, L. *J. Appl. Polym. Sci.* **2009**, *116*, 902.
7. Vav De Witte, P.; Dijkstra, P. J.; Van Den Berg, J. W. A.; Feijen J. *J. Polym. Sci. Part B: Polym. Phys.* **1996**, *34*, 2553.
8. Avella, M.; Errico, M. E.; Laurienzo, P.; Martuscelli, E.; Raimo, M.; Rimedio, R. *Polymer* **2000**, *41*, 3875.
9. Fujimaki, T. *Polym. Degrad. Stab.* **1998**, *59*, 209.
10. Song, J.; Ren, M.; Song, C.; Wang, S.; Zhang, H.; Mo, Z. *Polym. Int.* **2004**, *53*, 1773.
11. Liu, L.; Yu, J.; Cheng, L.; Qu, W. *Compos. Part A* **2009**, *40*, 669.
12. Song, L.; Qiu, Z. *Polym. Degrad. Stab.* **2009**, *94*, 632.
13. Bin, T.; Qu, J.p.; Liu, L.m.; Feng, Y.h.; Hu, S.x.; Yin, X.c. *Thermochim. Acta* **2011**, *525*, 141.
14. Ohkita, T.; Lee, S. H. *J. Appl. Polym. Sci.* **2005**, *97*, 1107.
15. Yoo, E. S.; Im, S. S. *J. Polym. Sci. Part B: Polym. Phys.* **1999**, *37*, 1357.
16. Yasuniwa, M.; Satou, T. *J. Polym. Sci. Part B: Polym. Phys.* **2002**, *40*, 2411.
17. Kong, Y.; Hay, J. N. *Polymer* **2003**, *44*, 623.
18. Yoshito, I.; Hideto, T. *Macromol. Rapid Commun.* **2000**, *21*, 117.
19. Dean, K.; Yu, L.; Bateman, S.; Wu, D. Y. *J. Appl. Polym. Sci.* **2007**, *103*, 802.
20. John, J.; Mani, R.; Bhattacharya, M. *J. Polym. Sci. Part A: Polym. Chem.* **2002**, *40*, 2003.

21. Ray, S. S.; Okamoto, K.; Maiti, P.; Okamotoa, M. *J. Nanosci. Nanotechnol.* **2002**, *2*, 1.
22. Okamoto, K.; Ray, S. S.; Okamoto, M. *J. Polym. Sci. Part B: Polym. Phys.* **2003**, *41*, 3160.
23. Utama, M. I. B.; Peng, Z.; Chen, R.; Peng, B.; Xu, X.; Dong, Y.; Wong, L. M.; Wang, S.; Sun, H.; Xiong, Q. *Nano Lett.* **2011**, *11*, 3051.
24. Ray, S. S.; Bandyopadhyay, J.; Bousmina, M. *Polym. Degrad. Stab.* **2007**, *92*, 802.
25. Busigin, C.; Lahtinen, R.; Martinez, G. M.; Thomas, G.; Woodhams, R. T. *Polym. Eng. Sci.* **1984**, *24*, 169.
26. Gan, D.; Lu, S.; Song, C.; Wang, Z. *Eur. Polym. J.* **2001**, *37*, 1359.
27. Ghannam, L.; Bacou, M.; Garay, H.; Shanahan, M. E. R.; François, J.; Billon, L. *Polymer* **2004**, *45*, 7035.
28. Maged, A. O.; Ayman, A.; Martin, M.; Ulrich, W. S. *Polymer* **2001**, *42*, 6545.
29. Malcom, F.; George, H. *Polym. Compos.* **1982**, *3*, 218.
30. Farzaneh, S.; Tcharkhtchi, A. *Int. J. Polymer. Sci.* **2011**, *2011*, 1.
31. Tomar, N.; Maiti, S. N. *J. Appl. Polym. Sci.* **2010**, *117*, 672.
32. Dipak, B.; De, P. P.; Golok, B. N. *Polym. Degrad. Stab.* **1999**, *65*, 47.
33. Ray, S. S.; Okamoto, M. *Macromol. Rapid Commun.* **2003**, *24*, 815.
34. Ray, S. S.; Okamoto, M. *Prog. Polym. Sci.* **2003**, *28*, 1539.
35. Ren, M.; Song, J.; Song, C.; Zhang, H.; Sun, X.; Chen, Q.; Zhang, H.; Mo, Z. *J. Polym. Sci. Part B: Polym. Phys.* **2005**, *43*, 3231.
36. Liu, X.; Li, C.; Xiao, Y.; Zhang, D.; Zeng, W. *J. Appl. Polym. Sci.* **2006**, *102*, 2493.
37. Chen, G. X.; Yoon, J. S. *J. Polym. Sci., Part B: Polym. Phys.* **2005**, *43*, 817.
38. Wu, M.; Yang, G.; Wang, M.; Wang, W.; Zhang, W. D.; Feng, J.; Liu, T. *Mater. Chem. Phys.* **2008**, *109*, 547.
39. Yang, Z.; Peng, H.; Wang, W.; Liu, T. *J. Appl. Polym. Sci.* **2010**, *116*, 2658.
40. Yeun, J. H.; Bang, G. S.; Park, B. J.; Ham, S. K.; Chang, J. H. *J. Appl. Polym. Sci.* **2006**, *101*, 591.
41. Avrami, M. *J. Chem. Phys.* **1939**, *7*, 1103.
42. Avrami, M. *J. Chem. Phys.* **1940**, *8*, 212.
43. Jeziorny, A. *Polymer* **1978**, *19*, 1142.
44. Ozawa, T. *Polymer* **1971**, *12*, 150.
45. Liu, T. X.; Mo, Z. S.; Zhang, H. F. *J. Appl. Polym. Sci.* **1998**, *67*, 815.
46. Vyazovkin, S.; Stone, J.; Sbirrazzuoli, N. *Macromol. Rapid Commun.* **2002**, *80*, 177.
47. Vyazovkin, S.; Sbirrazzuoli, N. *Macromol. Rapid Commun.* **2004**, *25*, 733.
48. Achilias, D. S.; Papageorgiou, G. Z.; Karayannidis, G. P. *Macromol. Chem. Phys.* **2005**, *206*, 1511.
49. Vyazovkin, S.; Sbirrazzuoli, N. *J. Phys. Chem. B* **2003**, *107*, 882.
50. Hwang, S. Y.; Ham, M. J.; Im, S. S. *Polym. Degrad. Stab.* **2010**, *95*, 1313.
51. Han, S.; Kang, S. W.; Kim, B. S.; Im, S. S. *Adv. Funct. Mater.* **2005**, *15*, 367.
52. Park, J. W.; Kim, D. K.; Im, S. S. *Polym. Int.* **2002**, *51*, 239.
53. Soccio, M.; Lotti, N.; Finelli, L.; Munari, A. *Eur. Polym. J.* **2009**, *45*, 171.